



Published in final edited form as:

*Neuropathology*. 2014 February ; 34(1): 11–18. doi:10.1111/neup.12055.

## Immunohistochemical analysis of ubiquilin-1 in the human hippocampus: Association with neurofibrillary tangle pathology

Katsuyoshi Mizukami<sup>1</sup>, Eric E. Abrahamson<sup>2,4</sup>, Zhiping Mi<sup>2</sup>, Masanori Ishikawa<sup>5</sup>, Kazushi Watanabe<sup>6</sup>, Setsuo Kinoshita<sup>6</sup>, Takashi Asada<sup>5</sup>, and Milos D. Ikonovic<sup>2,3,4</sup>

<sup>1</sup>Graduate School of Comprehensive Human Sciences, University of Tsukuba, 3-29-1 Otsuka, Bunkyo-ku, Tokyo 112-0012, Japan

<sup>2</sup>Department of Neurology, University of Pittsburgh, Pittsburgh, PA 15213, USA

<sup>3</sup>Department of Psychiatry, University of Pittsburgh, Pittsburgh, PA 15213, USA

<sup>4</sup>Geriatric Research Education and Clinical Center, V.A. Pittsburgh Healthcare System, Pittsburgh, PA 15213, USA

<sup>5</sup>Department of Psychiatry, Institute of Clinical Medicine, University of Tsukuba, 1-1-1 Tennodai, Tsukuba city, Ibaraki 305-8575, Japan

<sup>6</sup>Proubase Technology Inc. 1-525-1-102 Kosugi-machi, Nakahara-ku, Kawasaki-city, Kanagawa 211-0063, Japan

### Abstract

This postmortem immunohistochemical study examined the localization and distribution of ubiquilin-1 (UBL), a shuttle protein which interacts with ubiquitin and the proteasome, in the hippocampus from Alzheimer's disease (AD) dementia cases, and age-matched cases without dementia. Cases were stratified neuropathologically based on Braak staging for neurofibrillary tangles (NFT); cases without dementia were Braak stages 0-I-II (n=5), and AD cases were either Braak stages III-IV (n=7) or V-VI (n=11). In Braak stage 0-I-II cases, UBL immunoreactivity was detected in a dense fiber network in the neuropil, and in the cell cytoplasm and nucleoplasm of pyramidal neurons in CA fields and dentate gyrus granular neurons. In Braak stages III-IV and V-VI cases, UBL immunoreactivity was reduced in the neuropil and in the cytoplasm of the majority of CA1 neurons. In contrast, some CA1 pyramidal neurons and the majority of CA2/3 pyramidal, CA4 multipolar, and dentate granular neurons in Braak III-IV and Braak V-VI cases had markedly increased UBL immunoreactivity in the nucleoplasm. Dual immunofluorescence analysis of UBL and antibody clone AT8 revealed co-localization most frequently in CA1 pyramidal neurons in the Braak stage III-IV and V-VI cases. Further processing using the pan-amyloid marker X-34 revealed prominent UBL/X-34 dual labeling of extracellular NFT confined to the CA1/subiculum in the Braak stage V-VI cases. Our results demonstrate that in AD hippocampus, early NFT changes are associated with neuronal up-regulation of UBL in nucleoplasm, or its translocation from the cytoplasm to the nucleus. The perseverance of UBL

\*Address correspondence and reprint requests to: Katsuyoshi Mizukami, MD, PhD, Graduate School of Comprehensive Human Sciences, University of Tsukuba, 3-29-1 Otsuka, Bunkyo-ku, Tokyo 112-0012, Japan, Tel: +81-298-53-3210 fax: +81-298-53-3183 kmizukami@taiiku.tsukuba.ac.jp.

changes in CA2/3, CA4, and DG, generally considered as more resistant to NFT pathology, but not in the CA1, may mark a compensatory, potentially protective response to increased tau phosphorylation in hippocampal neurons; the failure of such a response may contribute to neuronal degeneration in end-stage AD.

## Keywords

Alzheimer; amyloid; Plic-1; ubiquilin; tau

---

## Introduction

The ubiquitin (Ub)–proteasome system is the major non-lysosomal proteolytic pathway in eukaryotes.<sup>1</sup> Ubiquilin-1 (also referred to as “protein linking integrin-associated protein to cytoskeleton 1”, or Plic-1) is a Ub-like (UBL) protein with functional domains on its N-terminus (UB) and C-terminus (Ub-associated; UBA). Ubiquilin interacts with polyubiquitylated proteins through its UBA domain and with two subunits of the 19S proteasome through the UB domain.<sup>2</sup> UBL protein is observed in neurofibrillary tangles (NFT) in Alzheimer’s disease (AD) brains<sup>3</sup>, facilitates presenilin synthesis<sup>3</sup>, and modulates amyloid precursor protein trafficking and amyloid-beta (A $\beta$ ) secretion.<sup>4</sup> Previous studies reported that early in AD, UBL-1 protein levels decrease in the frontal cortex<sup>5</sup>; the status of UBL-1 protein levels in the hippocampus in patients with varying degrees of NFT pathology is unknown. In this study, we used immunohistochemical techniques to examine localization and alterations in UBL-1 protein in the hippocampus from cases at different stages of NFT pathology as classified by Braak and Braak (1991)<sup>6</sup>. Multiple-label immunofluorescent microscopy analyses examined the relationship of UBL with early and late NFT changes. We hypothesized that changes in UBL-1 immunoreactivity intensity and/or cell type distribution are associated with the development and progression of NFT in AD hippocampus.

## Methods

Hippocampal tissue was obtained postmortem from 23 cases: 18 with a clinical diagnosis of probable AD and five age-matched cognitively intact cases without AD pathology or with NFT confined to the entorhinal cortex. Clinical diagnosis of AD was based on a standardized ADRC evaluation at a Consensus Conference, utilizing DSM-IV<sup>7</sup> and NINCDS/ADRDA<sup>8</sup> criteria. Demographic and neuropathology data are presented in Table 1. Neuropathological diagnosis was determined by a certified neuropathologist using CERAD<sup>9</sup> and NIA-Reagan Consensus criteria<sup>10</sup> (Table 1). All cases in the study were classified into stages 0 to VI according to Braak and Braak<sup>6</sup> (Table 1). One case (Braak stage IV) had a family history of AD.

Brain tissue was processed according to previously described procedures.<sup>11,12</sup> Blocks from the middle of the hippocampal body were cut in a coronal plane and placed in 0.1 M sodium phosphate buffer (PB, pH = 7.4) containing 4% paraformaldehyde for 48 h at 4°C and then cryoprotected by immersion in 30% sucrose in PB for no longer than seven days. The tissue was then frozen, sectioned at 40  $\mu$ m, and processed for immunohistochemistry as previously

described.<sup>11,12</sup> Sections were immunolabeled using a rabbit polyclonal antibody against ubiquilin 1 (U7258, Sigma, Lot# E0409, 1:1000), generated against an immunogen corresponding to carboxy terminus amino acids 502–519 of human ubiquilin-1. This antibody recognizes human ubiquilin-1 as a 62 kDa band on Western blot; this band is eliminated when the antibody is pre-incubated with the immunizing peptide (Sigma, manufacturer details). Furthermore, the immunoreactivity pattern observed using this antibody closely mirrors the pattern observed in a previous investigation of UBL-1 expression in AD brain<sup>3</sup>, both in the pattern of subcellular localization (cytoplasm and nucleoplasm; see below) and association with NFT (see below). Multiple labeling immunofluorescence was performed as described previously<sup>13</sup>. Sections were incubated overnight in a primary antibody cocktail consisting of rabbit anti-UBL (1:1,000; antibody specifics described above) and mouse monoclonal antibody clone AT8 (1:2,000; epitope on tau phosphorylated at Ser202<sup>14</sup>, Thermo Scientific, catalogue #MN1020, Lot #KK138691) in 1% normal goat serum for 24 hours at 4°C. Indirect immunofluorescence was achieved using a cocktail of goat anti-rabbit antisera conjugated to Alexa 488 (Molecular Probes, catalogue #A-11034, Lot #93C1-1) and goat anti-mouse antisera conjugated to Alexa 594 (Molecular Probes, catalogue #A-11032, Lot #93C1-1), both diluted 1:250 in 1% normal goat serum. Processed sections were mounted onto gelatin-coated slides and coverslipped with Fluoromount (SouthernBiotech). Immunofluorescent signal was detected using an Olympus BX53 upright microscope, the X-Cite 120Q excitation light source (Lumen Dynamics), an Olympus DP72 digital camera, and CellSens Standard 1.6 image acquisition software (Olympus). After initial analysis of UBL and AT8 immunofluorescence, slides were decoverslipped by immersion in PB, counterstained with the pan-amyloid binding dye, X-34, a highly fluorescent derivative of Congo red which detects NFT and A $\beta$  plaques with greater sensitivity than thioflavin-S,<sup>15,16</sup> and coverslipped with Vectashield Hard Set mounting medium with a DNA-specific fluorescent probe DAPI (Vector). Sections were then reanalyzed; X-34 did not interfere with either immunofluorescent marker signal, and was distinguished easily from the DAPI labeling of cell nuclei. Confirmation of fluorescence co-labeling of the four fluorescent markers was achieved using an Olympus BX51 upright microscope equipped with an Olympus DSU spinning disk confocal and motorized stage controlled by both StereoInvestigator (Version 8.0, MBF Bioscience) and SlideBook 4.2 (Intelligent Imaging Innovations) software, using Lumen200Pro metal halide illumination and a 60X 1.4 N.A. oil immersion objective. The four fluorescent markers were completely dissociable by color (UBL, AT8, X-34/DAPI) and subcellular localization (X-34, DAPI). Additional sections from each case were processed with cresyl violet to delineate the cytoarchitectural boundaries of the hippocampus as defined by Duvernoy<sup>17</sup>. Two independent evaluators determined intensity of the chromogen-based UBL immunoreactivity qualitatively on a scale from 0 (no immunoreactivity) to ++++ (most intense immunoreactivity, see Table 2). To reflect the variability in the immunoreactive signal between neurons in CA1 region of the Braak stage III–IV group, two scores are presented (Table 2). Quantification of chromogen-based UBL immunohistochemical optical density was performed as described previously<sup>18</sup> using Image J freeware.<sup>19</sup> Optical density was measured in the cytoplasm and nucleoplasm of pyramidal neurons in the CA1 and CA2/3 fields, and multipolar neurons in the CA4 field. Due to individual variation in overall intensity of UBL-ir between cases in each Braak staged group, analyses are presented as the

ratio of nucleoplasm-to-cytoplasm optical density values in the same sections/cases. Data was compared using the Kruskal Wallis test with Dunn's multiple comparison post hoc test, and Spearman rank order correlation tests, as the data did not conform to the prerequisites for parametric statistical testing. Significance values less than  $p = 0.01$  (non-directional) were considered statistically significant.

## Results

There were no statistically significant differences in demographics between the three Braak stage groups although the Braak stage 0-I-II (non-AD) group trended towards younger age ( $p = 0.013$  by Kruskal-Wallis, no differences were detected with Dunn's multiple comparison test). UBL immunoreactivity had distinct patterns in the three Braak stage groups (described below), and localization was almost exclusively neuronal in all groups, with only in 2/11 cases (one Braak stage VI, one Braak stage IV with family history of AD) exhibiting UBL immunoreactivity in cells with the morphological appearance of microglia and oligodendrocytes, and located throughout the gray and white matter, respectively (not shown). In Braak stage 0-I-II cases (NFT absent or confined to the entorhinal cortex), UBL immunoreactivity was observed in the neuropil in the stratum pyramidale of the Ammon's horn (CA) and molecular layer of the dentate gyrus (DG). UBL immunoreactivity was also detected in neuronal soma, dendrites, and in the nucleoplasm in hippocampal neurons, including pyramidal and multipolar neurons in the CA fields, and DG granular neurons. In the majority of neurons, UBL immunoreactivity intensity was higher in the nucleoplasm compared to the cytoplasm (Figure 1; Table 2). UBL immunoreactivity in the nucleoplasm appeared punctuate/vesicular (Figure 1 inset a; Figure 4A) and was most prominent in the CA2/3 field (Table 2).

In Braak stage III-IV cases (NFT involving the entorhinal cortex and hippocampus but not neocortex), UBL immunoreactivity in the neuropil was reduced in the CA1 and CA2/3 regions, and was unchanged in the CA4 and DG, compared to Braak stage 0-I-II cases. The majority of CA1 neurons exhibited reduced cytoplasmic and nucleoplasmic labeling, however a subset of CA1 pyramidal neurons had prominent UBL immunoreactivity in the nucleoplasm (Figure 1B). The intensity of UBL immunoreactivity in the nucleoplasm increased markedly in the majority of CA2/3 pyramidal neurons, CA4 multipolar neurons, and DG granular neurons (Figure 1E; 2 H,K; Table 2). We also observed UBL immunoreactivity in fibers in the CA2/3 radiatum/moleculare and DG molecular layer in three of the Braak stage III-IV cases (Braak III: 1; Braak IV: 2; not shown).

In Braak stage V-VI cases, UBL immunoreactivity was less intense in the CA1 field, both in the neuropil and in pyramidal neurons, except those with the morphological appearance of extracellular NFT (eNFT), where UBL immunoreactivity was prominent (Figure 1C. inset c). In contrast, UBL immunoreactivity in neuropil and neuronal cytoplasm in CA2/3, CA4, and dentate gyrus was similar to the pattern observed in Braak stage III-IV cases, albeit with a less prominent increase in nucleoplasmic UBL immunoreactivity (Figure 1F,I,L; Table 2).

Analysis of UBL immunoreactivity optical density confirmed a significant increase ( $p < 0.0001$ ) in the nucleoplasm/cytoplasm optical density ratio in the CA1 field from Braak

stages 0-I-II compared to Braak stages III-IV (Figure 2; in Braak stages V-VI, small numbers of UBL immunoreactive pyramidal cells remaining in the CA1 precluded optical density analyses). The ratio was slightly, but non-significantly, elevated in the CA2/3 field from Braak stage groups III-IV and V-VI when compared to Braak stage group 0-I-II, and a similar trend was observed in the CA4 field (Figure 2). Optical density measurements in the nucleoplasm and cytoplasm correlated directly across all Braak staged groups in CA2/3 as well as in CA4, but did not correlate in the CA1 field (data not shown). We detected statistically significant (Spearman  $r = 0.7$ ,  $p = 0.01$ ) correlation between more advanced age and higher nucleoplasm/cytoplasm UBL immunoreactivity optical density ratio values in CA1, but not CA2/3 or CA4.

The relationship between UBL protein and a marker of advanced stage NFT including extracellular “ghost NFT” (X-34) or an antibody that also recognizes pre/early NFT (AT8) was examined using multiple-label fluorescence confocal microscopy (Figures 3, 4). The pattern of UBL immunofluorescence was consistent with our observations using the same antibody and chromogen-based immunohistochemistry with light microscopy (Figure 3). In multiple-labeled (UBL, AT8, DAPI, X-34) sections from Braak stage 0-I-II cases, we observed pyramidal neurons with UBL-immunofluorescence in the cytoplasm and nucleoplasm, the latter co-labeled with DAPI (Figure 3A-D). Braak 0-I-II cases had no AT8 or X-34 positive NFT in the hippocampus, though sparse, scattered AT8 immunofluorescent neuritic elements were observed in the CA fields (Figure 3E-H). In Braak staged III-IV and V-VI cases, we observed a complex pattern of UBL/AT8 or UBL/X-34 co-localization in CA fields. Neurons with light cytoplasmic and prominent nucleoplasmic UBL immunofluorescence co-localized AT8, but had little or no X-34, (Figure 3I-L, M-P, M'-P'). The majority of UBL-immunofluorescent pyramidal neurons in the CA2/3 region were AT8- and X34-negative, yet surrounded by numerous AT8-immunofluorescent neurites (Figure 3I-L). Pyramidal neurons in CA1 and subiculum of Braak staged V-VI cases had UBL immunofluorescence co-localized with X-34, and very little or no AT8 immunofluorescence and no DAPI labeling, indicative of extracellular ‘ghost’ NFT (eNFT, Figure 3M-P, M''-P''). UBL immunoreactive neuritic elements were also detected within X-34 labeled amyloid plaques in the CA1 and DG molecular layer (not shown). A small number of AT8 positive neurons lacking UBL immunofluorescence were observed in the CA1 region of Braak V-VI cases. The overall pattern of UBL/AT8/X-34 immunofluorescence in a representative Braak stage VI case is illustrated diagrammatically in Figure 4.

## Discussion and Conclusion

The present study investigated UBL immunoreactivity in the hippocampus from non-AD and clinically-diagnosed AD cases stratified by Braak stages, in relation to markers of primarily advanced stage NFT (the pan-amyloid marker X-34) and the antibody clone AT8 which also recognizes pre/early NFT. We report two novel findings: 1) with the emergence of NFT in the hippocampus, UBL immunoreactivity in pyramidal neurons changes from cytoplasmic/nuclear to predominantly nuclear localization and, in a subset of neurons, co-localizes with phosphorylated tau and 2) prominent UBL immunoreactivity is present in a subset of end-stage, extracellular NFT (eNFT) in the CA1/subiculum. Neurons in CA2-4

fields and DG, generally spared from classic NFT pathology development in AD, exhibited markedly increased UBL immunoreactivity in the nucleoplasm in Braak stages III–IV and V–VI AD cases compared to the Braak 0-I-II group. The reason for this change is unknown, but it may be influenced by age differences between Braak groups, since the Braak stage 0-I-II (non-AD) group trended towards being younger than both the Braak stage III–IV and Braak stage V–VI AD groups. Other factors, including nucleotide polymorphisms in the ubiquilin gene, may contribute to the observed differences and warrant future clinical-genetic-pathological studies. Genetic abnormalities in UBL-1 were reported to associate with increased risk<sup>20</sup> and age of onset and duration<sup>21</sup> of AD, although this association was not replicated in all studies.<sup>22</sup> Because Braak staged groups represent a continuum, rather than a stepwise progression, of NFT pathology, the large variability in UBL intensity ratios in the Braak stage III–IV group, particularly in the CA1 region, is likely due to variability in the extent of pathologic changes, and UBL expression, in individual pyramidal neurons.

The functional relevance of the changes in the subcellular localization of UBL, and their association with different types of NFT, is unknown but it may reflect a response, compensatory or dysregulatory, of the ubiquitin-proteasome system to increased cellular stress due to accumulation of aggregated and heavily-phosphorylated proteins, especially tau. Our observation of increased UBL immunoreactivity in X-34 positive eNFT is particularly intriguing considering that ubiquitin, a major component of NFT's paired helical filaments in AD,<sup>23,24</sup> is largely absent from eNFT.<sup>23, 25, 26</sup> These changes may occur in relation to ubiquitin-proteasome dysfunction or, alternatively, they may reflect altered antigenic profiles of these proteins in eNFT.<sup>27</sup> The observation of UBL immunoreactivity in X-34 positive neuritic plaques in advanced Braak stages further suggests a relationship between UBL and tau changes, and warrants further exploration. Furthermore, the source of the fibers that comprise UBL immunoreactive dystrophic neurites, and the significance of these changes in the pathogenesis of neuritic plaques, is unknown. Further investigation is also warranted regarding the observation of UBL immunoreactive cells with the morphological appearance of microglia and oligodendrocytes in the hippocampus of two AD cases, especially when considering that one case had a family history of AD. Ubiquilin is up-regulated in glial cells in some pathologic conditions including hypoxia,<sup>28</sup> thus glial cells could increase ubiquilin 1 expression due to cell stress induced by neurofibrillary pathology. Alternatively, these observations may be indicative of differences in subjects' agonal state.

In conclusion, these results demonstrate that in AD hippocampus, UBL immunoreactivity increases in the neuronal nucleoplasm and is associated with region-specific neurofibrillary changes. Up-regulation of UBL could contribute to pathology progression, or reflect a compensatory response. Future studies examining the link between UBL and NFT as well as other types of AD pathology are warranted.

## Acknowledgments

We are indebted to the support of the participants in the ADRC at the University of Pittsburgh. This study was supported by NIH grants NIA AG05133 (University of Pittsburgh ADRC), AG014449 and AG025204 (MDI), The Snee-Reinhardt Charitable Foundation (MDI), and by a Grant-in-Aid for Scientific Research from the Japanese Ministry of Education, Culture, Sports, Science and Technology (KM). Ms. Suganya Srinivasan, Ms. Lan Shao, Ms. Natsuko Kato and Ms. Megumi Mitani provided expert technical assistance.



## References

1. Hershko A, Ciechanover A. The ubiquitin system. *Annu Rev Biochem.* 1998; 67:425–479. [PubMed: 9759494]
2. Ko HS, Uehara T, Tsuruma K, Nomura Y. Ubiquilin interacts with ubiquitylated proteins and proteasome through its ubiquitin-associated and ubiquitin-like domains. *FEBS Letters.* 2004; 566:110–114. [PubMed: 15147878]
3. Mah AL, Perry G, Smith MA, Monteiro MJ. Identification of ubiquilin, a novel presenilin interactor that increases presenilin protein accumulation. *J Cell Biol.* 2000; 151:847–862. [PubMed: 11076969]
4. Hiltunen M, Lu A, Thomas AV, et al. Ubiquilin 1 modulates amyloid precursor protein trafficking and A $\beta$  secretion. *J Biol Chem.* 2006; 281:32240–32253. [PubMed: 16945923]
5. Stieren ES, El Ayadi A, Xiao Y, et al. Ubiquilin-1 is a molecular chaperone for the amyloid precursor protein. *J Biol Chem.* 2011; 286:35689–35698. [PubMed: 21852239]
6. Braak H, Braak E. Neuropathological staging of Alzheimer-related changes. *Acta Neuropathol (Berl).* 1991; 82:239–259. [PubMed: 1759558]
7. American Psychiatric Association. *Diagnostic and statistical manual of mental disorders.* 4. Washington, D.C: American Psychiatric Association; 1994.
8. McKhann G, Drachman D, Folstein M, Katzman R, Price D, Stadlan EM. Clinical diagnosis of Alzheimer's disease: Report of Health and Human Services Task Force on Alzheimer's disease. *Neurology.* 1984; 34:939–944. [PubMed: 6610841]
9. Mirra SS, Heyman A, McKeel D, et al. The consortium to establish a registry for Alzheimer's disease (CERAD). Part II. Standardization of the neuropathologic assessment of Alzheimer's disease. *Neurology.* 1991; 41:479–486. [PubMed: 2011243]
10. Consensus report of the Working Group on "Molecular and Biochemical Markers of Alzheimer's Disease". The Ronald and Nancy Reagan Research Institute of the Alzheimer's Association and the National Institute on Aging Working Group. *Neurobiol Aging.* 1998; 19:109–116. [PubMed: 9558143]
11. Mizukami K, Ikonovic MD, Grayson DR, et al. Immunohistochemical study of GABAA receptor  $\beta$ 2/3 subunits in the hippocampal formation of aged brains with Alzheimer-related neuropathologic changes. *Exp Neurol.* 1997; 147:333–345. [PubMed: 9344558]
12. Iwakiri M, Mizukami K, Ikonovic MD, et al. An immunohistochemical study of GABA receptor gamma subunits in Alzheimers disease hippocampus: relationship to neurofibrillary tangle progression. *Neuropathology.* 2009; 29:263–269. [PubMed: 19019179]
13. Ikonovic MD, Abrahamson EE, Uz T, Manev H, Dekosky ST. Increased 5-lipoxygenase immunoreactivity in the hippocampus of patients with Alzheimer's disease. *J Histochem Cytochem.* 2008; 56:1065–1073. [PubMed: 18678882]
14. Mercken M, Vandermeeren M, Lübke U, et al. Monoclonal antibodies with selective specificity for Alzheimer Tau are directed against phosphatase-sensitive epitopes. *Acta Neuropathol.* 1992; 84:265–272. [PubMed: 1384266]
15. Styren SD, Hamilton RL, Styren GC, Klunk WE. X-34, a fluorescent derivative of Congo red: a novel histochemical stain for Alzheimer's disease pathology. *J Histochem Cytochem.* 2000; 48:1223–1232. [PubMed: 10950879]
16. Ikonovic MD, Abrahamson EE, Isanski BA, et al. X-34 labeling of abnormal protein aggregates during the progression of Alzheimer's disease. *Methods Enzymol.* 2006; 412:123–144. [PubMed: 17046656]
17. Duvernoy, HM. *The Human Hippocampus.* Munchen: JF Bergmann Verlag; 1988.
18. Iwakiri M, Mizukami K, Ikonovic MD, et al. Changes in hippocampal GABABR1 subunit expression in Alzheimer's patients: association with Braak staging. *Acta Neuropathol.* 2005; 109:467–474. [PubMed: 15759131]
19. Rasband, WS. *ImageJ.* U. S. National Institutes of Health; Bethesda, Maryland, USA: 1997–2012. <http://imagej.nih.gov/ij/>
20. Bertram L, Hiltunen M, Parkinson M, et al. Family-based association between Alzheimer's disease and variants in UBQLN1. *N Engl J Med.* 2005; 352:884–894. [PubMed: 15745979]

21. Kamboh MI, Minster RL, Feingold E, DeKosky ST. Genetic association of ubiquilin with Alzheimer's disease and related quantitative measures. *Mol Psychiatry*. 2006; 11:273–279. [PubMed: 16302009]
22. Smemo S, Nowotny P, Hinrichs AL, et al. Ubiquilin 1 polymorphisms are not associated with late-onset Alzheimer's disease. *Ann Neurol*. 2006; 59:21–26. [PubMed: 16278862]
23. Mori H, Kondo J, Ihara Y. Ubiquitin is a component of paired helical filaments in Alzheimer's disease. *Science*. 1987; 235:1641–1644. [PubMed: 3029875]
24. Perry G, Friedman R, Shaw G, et al. Ubiquitin is detected in neurofibrillary tangles and senile plaque neurites of Alzheimer disease brains. *Proc Natl Acad Sci U S A*. 1987; 84:3033–3036. [PubMed: 3033674]
25. Ikeda K, Haga C, Oyanagi S, et al. Ultrastructural and immunohistochemical study of degenerate neurite-bearing ghost tangles. *J Neurol*. 1992; 239:191–194. [PubMed: 1597685]
26. Kobayashi K, Muramori F, Aoki T, et al. KP-1 is a marker for extraneuronal neurofibrillary tangles and senile plaques in Alzheimer diseased brains. *Dement Geriatr Cogn Disord*. 1998; 9:13–19. [PubMed: 9469259]
27. Bancher C, Brunner C, Lassmann H, et al. Tau and ubiquitin immunoreactivity at different stages of formation of Alzheimer neurofibrillary tangles. *Prog Clin Biol Res*. 1989; 317:837–848. [PubMed: 2557644]
28. Ko HS, Uehara T, Nomura T. Role of ubiquilin associated with protein-disulfide isomerase in the endoplasmic reticulum in stress-induced apoptotic cell death. *J Biol Chem*. 2002; 277:35386–35392. [PubMed: 12095988]



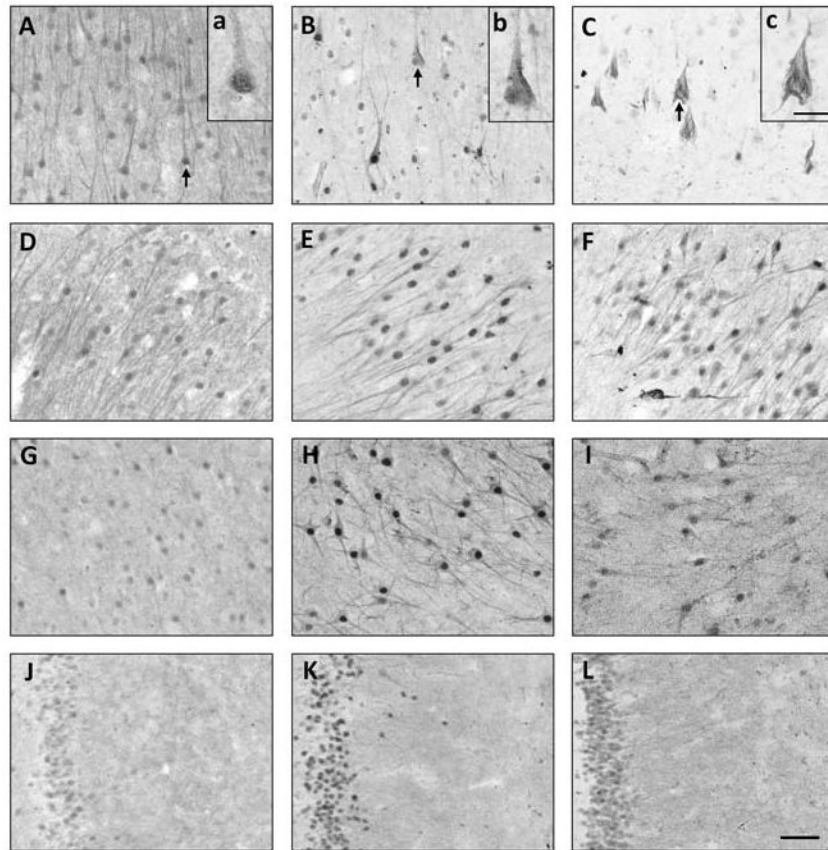


**Fig. 1.**

Photomicrographs showing ubiquitin (UBL) immunoreactivity in CA1 (A–C), CA2/3 (D–F), CA4 (G–I), and dentate gyrus (J–L; molecular layer is on the right) hippocampal fields in cases representative of Braak stages 0–I–II (A, D, G, J), Braak stages III–IV (B, E, H, K), and Braak stages V–VI (C, F, I, L) groups. In the CA1 field, representative UBL-ir pyramidal neurons (arrows) are illustrated at a higher magnification in the insets (a–c). Scale bar = 50  $\mu$ m (A–L); 20  $\mu$ m (a–c).

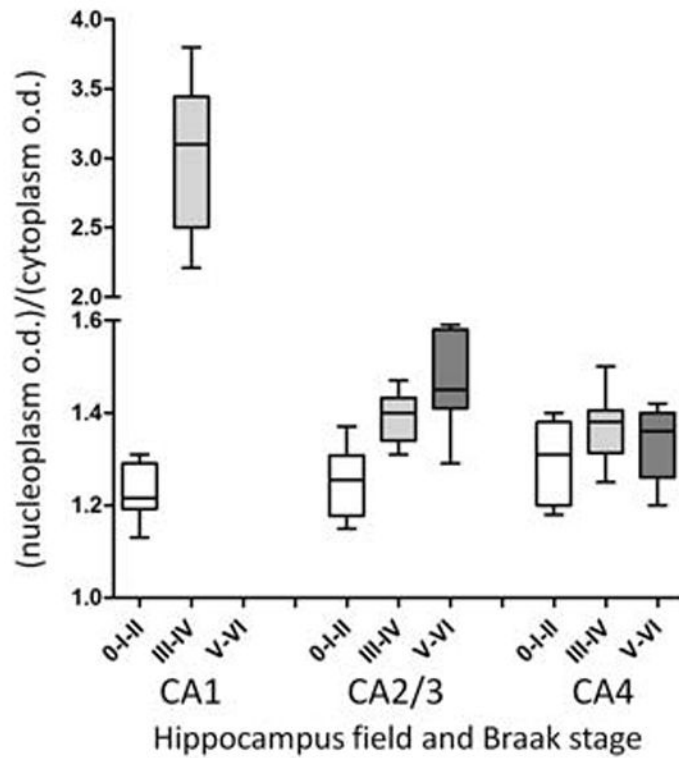


**Fig. 2.**

Box and whiskers graphs represent results from optical density measurements of ubiquitin-immunohistochemistry in the CA1, CA2/3, and CA4 hippocampus fields in cases with Braak stages 0-I-II, III-IV, and V-VI. Due to high variability in the intensity of UBL-immunoreactivity across cases, data were expressed as a ratio of the values obtained from the nucleoplasm and cytoplasm. There were insufficient pyramidal neurons in CA1 hippocampus in Braak group staged V-VI to perform the analysis. Box plots describe the following: whiskers, maximum and minimum values; line within box, median; upper and lower limits of box, upper and lower quartiles.

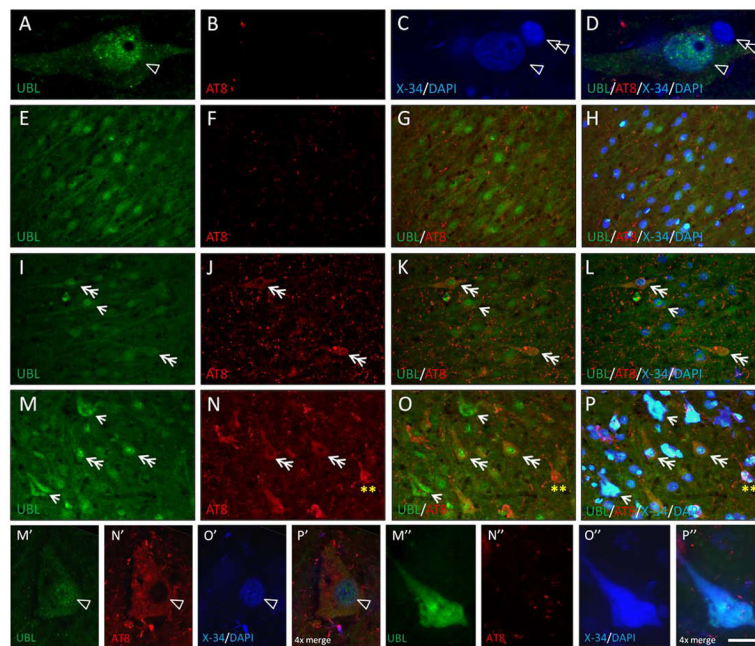


**Fig. 3.**

Multiple-label fluorescent microscopy analyses of associations between ubiquilin (UBL) and markers of NFT (antibody clone AT8 and amyloid dye X-34). A–D: Confocal imaging of UBL immunofluorescence (A, green) in the nucleoplasm and cytoplasm of a large pyramidal neuron in the CA1 region of the hippocampus from a Braak stage I case. The nucleoplasm is co-labeled with the DNA binding compound 4',6-diamidino-2-phenylindole (C, D, single arrowhead; DAPI). The nucleus of an adjacent glial cell is also prominently DAPI-labeled but it lacks UBL immunoreactivity (C,D, double arrowhead). There are only small amounts of AT8 immunofluorescence and X-34 histofluorescence in some neuritic processes, but not in neuronal cell bodies (B,D). E–H: UBL immunofluorescence (E,G,H green) in the nucleoplasm and cytoplasm of neurons in the CA3 region of the hippocampus from a Braak stage II case. AT8-immunofluorescence is scarce, restricted to neurites scattered in the neuropil (F–H, red). UBL-immunofluorescent neurons exhibit prominent nuclear labeling with DAPI (H). No X-34 positive tangles are present (H). I–L: UBL immunofluorescence (I,K,L, green) in the nucleoplasm and cytoplasm of neurons in the CA3 region of the hippocampus from a Braak stage IV case. AT8-immunofluorescence is observed in neurites (J–L red) scattered in the neuropil and in the cytoplasm of some pyramidal neurons (J, double arrowheads); these neurons are co-labeled with UBL in the cytoplasm and nucleoplasm (K, double headed arrows). A UBL positive cell that lacks AT8 labeling is indicated by an arrow. UBL and UBL/AT8 immunofluorescent neurons are co-labeled with DAPI but do not contain X-34 histofluorescence (L). M–P: UBL immunofluorescence (M, O, P, green) in the CA1 region of the hippocampus from a Braak stage VI case, co-labeled with AT8 (O), DAPI and X-34 (P, all four markers merged). UBL and AT8 co-localize in the cytoplasm of a subset of neurons which contain UBL (and DAPI) positive nucleus but are devoid of X-34 signal (P; double arrows). UBL is detectable in a subset of X-34 positive extracellular NFT (NFT lacking detectable nucleus) that exhibit little, if any, AT8 signal (M,O,P; arrows). AT8 positive intracellular NFT with no detectable UBL immunofluorescence are also detected (N–P; double asterisk). M'–P': Confocal microscopic image of UBL immunofluorescence in the cytoplasm and nucleoplasm (M', green) of an AT8-positive intracellular NFT with DAPI-confirmed nucleus (O'–P') in the CA1. M''–P'': Confocal microscopic image of UBL immunofluorescence (M'', green) in an extracellular NFT (devoid of DAPI signal) with prominent X-34 co-labeling (O''–P'') and very little AT8 signal (N'') in the CA1. Scale bar = 7  $\mu$ m (A–D), 40  $\mu$ m (E–H), 30  $\mu$ m (I–P), 14  $\mu$ m (M'–P'').

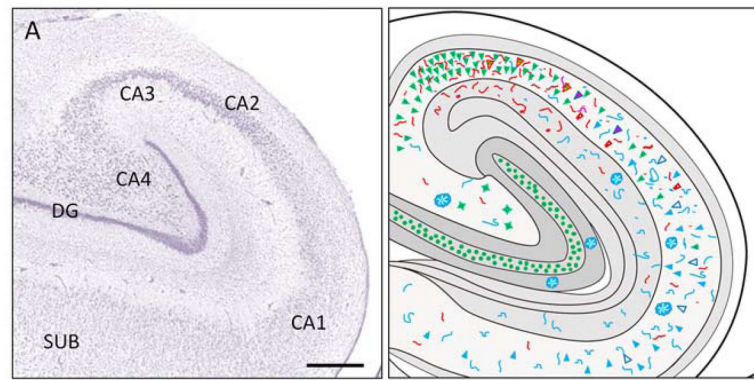


**Fig. 4.**

A. Sub-regional division of the hippocampus illustrated in a Nissl stained section. CA1, CA2, CA3, CA4 = Cornu Ammonis fields 1–4; DG = dentate gyrus, SUB = subiculum. Scale bar = 200  $\mu$ m. B. Schematic illustration of the pattern of ubiquilin, AT8, and X-34 fluorescence in the hippocampus from a representative Braak stage VI case.

UBL + pyramidal cell	UBL/AT8	AT8 + pre-amyloid	AT8/NFT	
AT8/X-34 + NFB4 + extracellular	UBL/X-34	AT8	extracellular NFT	
UBL + CA4	UBL + granule cell	UBL + nucleus		
AT8 + neurites	X-34 + NFB4	X-34 + amyloid plaque	with X-34/UBL/A'	

**Table 1**

Case demographic data.

Demographic	Braak stage 0-I-II	Braak stage III-IV	Braak stage V-VI
<b>Number of cases</b>			
(N)	3-1-1	3-4	4-7
<sup>1</sup> Age (years)			
Mean (SD)	61.4 (9)	78.5 (7.2)	75.2 (10.5)
Range	48-71	68-90	63-91
<b>CERAD diagnosis</b>	Not AD (5)	Probable (7)	Definite (11)
<sup>2</sup> NIA-Reagan diagnosis	Low (5)	Intermediate (7)	High (11)
<b>Brain weight (g)</b>			
Mean (SD)	1120 (346.3)	1192 (161.7)	1110 (137.9)
Range	690-1600	970-1350	930-1300
<b>PMI (hours)</b>			
Mean (SD)	5.8 (1.5)	6 (2.5)	6.5 (2.7)
Range	4-8	2-9	2-17
<b>Sex</b>			
(Male)	1-0-1	2-3	1-2
<b>A<math>\beta</math> deposits</b>			
(Present)	0-0-1	3-4	4-7
<sup>3</sup> Co-neuropsychiatric			
(Present)	0-0-1	0-0	2-4
<sup>4</sup> Co-pathology			
(Present)	3-0-0	1-2	0-1
<b>Race</b>			
(White)	2-1-1	2-4	4-7

<sup>1</sup> p = 0.013 (Kruskal-Wallis); p < 0.01 (Dunn's multiple comparison test).

<sup>2</sup> Likelihood of Alzheimer's disease

<sup>3</sup> Braak stage 0-I-II: Frontotemporal dementia; Braak stage V-VI: abuse (V – indicates Braak stage), delusions (V, VI, VI), depression (V, VI) (all separate).

<sup>4</sup> Braak stage 0-I-II: Pick's disease (0), Corticobasal degeneration (0), MND-inclusion dementia (0) (all separate); Braak stage III-IV: DLB mild (III), DLB severe (IV, IV); Braak stage V-VI: DLB severe (VI).

**Abbreviations:** A $\beta$ , amyloid-beta peptide; DLB, Lewy bodies; g, grams; MND, motor neuron disease; N, number of subjects; PMI, post mortem interval; SD, standard deviation.

**Table 2**

Qualitative analysis of ubiquitin-1 immunoreactivity intensity in the hippocampus from cases staged Braak 0-I-II, III-IV, and V-VI).

	NEUROFIL				NEURONAL CYTOPLASM				NEURONAL NUCLEOPLASM			
	CA1	CA2/3	CA4	DG	CA1	CA2/3	CA4	DG	CA1	CA2/3	CA4	DG
Braak 0-I-II	++	++	++	+	++	++	+	+	++	+++	++	+
Braak III-IV	+	+	++	+	0/+	++	++	++	+	++++	++++	++
Braak V-VI	+	+	++	+	+	+	+	++	+	+++	+++	++